Integrated, Stretched, and Adiabatic Solid Effects

Yifan Quan,
Francis Bitter Magnet Laboratory and Department of Chemistry, Massachusetts Institute of Technology, Cambridge, Massachusetts 02139, United States

Jakob Steiner,
Paul Scherrer Institute (PCI), 5232 Villigen, Switzerland

Yifu Ouyang,
Francis Bitter Magnet Laboratory and Department of Chemistry, Massachusetts Institute of Technology, Cambridge, Massachusetts 02139, United States

Kong Ooi Tan,
Francis Bitter Magnet Laboratory and Department of Chemistry, Massachusetts Institute of Technology, Cambridge, Massachusetts 02139, United States; Currently at Laboratoire des Biomolécules, LBM, Département de Chimie, École Normale Supérieure, PSL University, Sorbonne Université, CNRS, 75005 Paris, France

W. Thomas Wenckebach,
Paul Scherrer Institute (PCI), 5232 Villigen, Switzerland; National High Magnetic Field Laboratory, University of Florida, Gainesville, Florida 32310, United States

Patrick Hautle,
Paul Scherrer Institute (PCI), 5232 Villigen, Switzerland

Robert G. Griffin
Francis Bitter Magnet Laboratory and Department of Chemistry, Massachusetts Institute of Technology, Cambridge, Massachusetts 02139, United States

Abstract

This paper presents a theory describing the dynamic nuclear polarization (DNP) process associated with an arbitrary frequency swept microwave pulse. The theory is utilized to explain the integrated solid effect (ISE) as well as the newly discovered stretched solid effect (SSE) and adiabatic solid effect (ASE). It is verified with experiments performed at 9.4 GHz (0.34 T) on single crystals of naphthalene doped with pentacene-d_{14}. It is shown that the SSE and ASE can be more efficient than the ISE. Furthermore, the theory predicts that the efficiency of the SSE improves at high magnetic fields, where the EPR line width is small compared to the nuclear Larmor frequency. In

Corresponding Author: Robert G. Griffin – rgg@mit.edu.

The authors declare no competing financial interest.

Complete contact information is available at: https://pubs.acs.org/10.1021/acs.jpclett.2c01147

ASSOCIATED CONTENT
Supporting Information
The Supporting Information is available free of charge at https://pubs.acs.org/doi/10.1021/acs.jpclett.2c01147.
Transparent Peer Review report available (PDF)

addition, we show that the ISE, SSE, and ASE are based on similar physical principles and we suggest definitions to distinguish among them.

Graphical Abstract

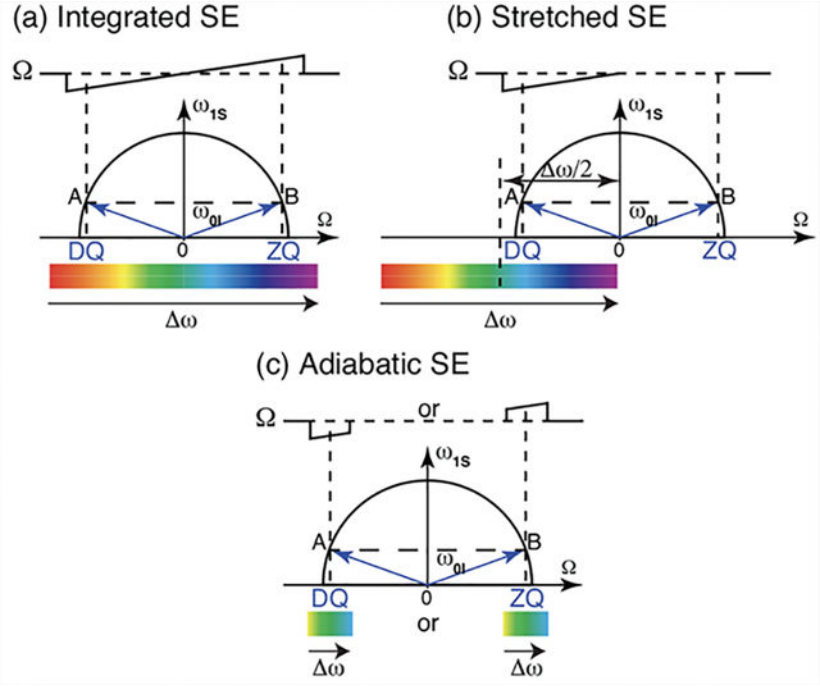

The sensitivity of magnetic resonance experiments is the factor that chronically limits the success of any application. As a consequence, each advance in methodology and technology that has improved signal-to-noise in nuclear magnetic resonance (NMR), electron paramagnetic resonance (EPR) and magnetic resonance imaging (MRI) has erased existing scientific boundaries and initiated new areas of application and directions of research. A prominent example is dynamic nuclear polarization (DNP) that, in the past decade, has evolved in several guises as the method of choice for NMR signal enhancement.

However, in what are now routine continuous wave (CW) DNP experiments—the solid effect (SE) or cross-effect (CE)—the signal enhancement factor, ε, exhibits a dependence on the nuclear Larmor frequency $\sim\omega_{0I}^{-1}$ to $\sim\omega_{0I}^{-2}$. Therefore, when experiments are performed at high magnetic fields, which are essential to optimize NMR spectral resolution, signal enhancements drop significantly. In contrast, time domain or pulsed DNP mechanisms should not display an ω_{0I} dependence and thus provide a promising approach to enhance sensitivity in acquisition of high field NMR spectra.

One of the most favorable time domain DNP methods is the integrated solid effect (ISE), which was initially performed by sweeping the magnetic field through the SE matching conditions within the electron spin coherence time.[1,2] When the sweep is adiabatic, the polarization is coherently transferred from the electron to the surrounding nuclei. However, at high magnetic fields (9–28 T) where most NMR is currently performed, it is technically

challenging to rapidly sweep the Zeeman field, B_0. Alternatively, the Q of the microwave circuit is small, and therefore, the microwave frequency can be modulated with an arbitrary waveform generator (AWG)[3–5] or a frequency agile gyrotron[6,7] while keeping the magnetic field constant. Using this approach, it has been shown that the ISE can be as efficient as nuclear orientation via electron spin locking (NOVEL),[8,9] the gold standard DNP mechanism. Concurrently, the ISE requires much less microwave power than NOVEL,[4] making it a promising method for high field experiments.

In addition to the ISE, two closely related chirped pulse experiments were recently developed. First, in performing experiments where the chirped frequency is not centered on the EPR spectrum, we observed a new polarization mechanism the stretched solid effect (SSE).[4] Second, when the chirped pulse is swept across one of the solid effect (SE) transitions at $\omega_{0S} \pm \omega_{0I}$ the signals were enhanced by a factor of ~2.4 over the SE enhancement, an effect we term an adiabatic solid effect (ASE).[10] Figure 1 illustrates the frequency modulation schemes of all three of these experiments—the ISE, SSE, and ASE. Furthermore, although it was observed experimentally that the SSE and ASE can be more efficient than a full ISE sweep, a theoretical understanding of this observation and these two DNP mechanisms is not yet available. Finally, the intellectual boundaries among the ISE, SSE, and ASE are not well-defined. This situation provides the motivation for the development of a comprehensive theory for arbitrary chirped pulse DNP, which will clarify the polarization transfer mechanism of these three DNP methods and hopefully lead to their further improvement.

To calculate the polarization transfer of an arbitrary chirped pulse, we employ the Landau–Zener theory and single value decomposition theories that were used previously to describe the ISE.[2] We consider a spin system consisting of a single electron spin S interacting with N_I nuclear spins I, as the electron spin is typically very dilute. In addition, we neglect the internuclear dipolar interaction because it is much weaker than the electron–nuclear dipole coupling and not involved in the direct polarization transfer process. The internuclear dipolar coupling is essential for spin diffusion, which is a secondary process after the polarization transfer and is required for the DNP process to polarize the bulk nuclei.

Assuming an adiabatic sweep from $-\infty$ and an initial nuclear polarization, $P_I = 0$, the electron polarization after matching point A and subsequently point B are written down using eqs 70 and 72 from Henstra et al.[2]

$$P_S^{\mathrm{A}} = \int_0^\infty \mathrm{d}\sigma^2\, g\left(\sigma^2\right) P_S^0(2\mathscr{P} - 1) = P_S^0 \frac{1 - \mathscr{Q}}{1 + \mathscr{Q}} \tag{1}$$

and

$$\begin{aligned} P_S^{\mathrm{B}} &= \int_0^\infty \mathrm{d}\sigma^2\, g\left(\sigma^2\right) P_S^0(2\mathscr{P} - 1)^2 \\ &= P_S^0\left(1 - \frac{4}{(1 + 2\mathscr{Q})(1 + \mathscr{Q}^{-1})}\right) \end{aligned} \tag{2}$$

Here, P_S^0 denotes the initial electron polarization, σ the hyperfine interaction strength with a spectral density $g(\sigma^2) = \frac{1}{M_2}\exp\left(-\frac{\sigma^2}{M_2}\right)$ where M_2 is the second moment, and

$$\mathscr{P} = \exp\left(-2\pi\frac{\sin^2\theta_A\sigma^2}{|\cos\theta_A\dot{\omega}|}\right) \tag{3}$$

where $\sin\theta_A = \omega_{1S}/\omega_{0I}$ denotes the extent of state mixing and $\dot{\omega}$ is the rate of the frequency sweep. Furthermore

$$\mathscr{Q} = 2\pi\frac{\sin^2\theta_A M_2}{|\cos\theta_A\dot{\omega}|} \tag{4}$$

Notice that $\mathscr{P}$ and $\mathscr{Q}$ are derived from the Landau–Zener theory and the definition of $\mathscr{Q}$ here is different by a factor of $\sqrt{2}$ from that defined by Henstra et al.[2] In addition, the sweep needs to be adiabatic, i.e., $\frac{\pi\omega_{1S}^2}{2|\dot{\omega}|} \gg 1$ otherwise the polarization transfer is inefficient.

From (1) and (2) we can write down the polarization transfer efficiency, E_{SSE} and E_{ISE}, for a given nuclear polarization P_I,

$$E_{SSE} = \frac{P_S^0 - P_S^A}{P_S^0 - P_I} = \frac{2\mathscr{Q}}{1+\mathscr{Q}} \tag{5}$$

and

$$E_{ISE} = \frac{P_S^0 - P_S^B}{P_S^0 - P_I} = \frac{4}{(1+2\mathscr{Q})(1+\mathscr{Q}^{-1})} \tag{6}$$

These quantities are plotted in Figure 2. It should be pointed out that the efficiency E_{ISE} for a full ISE has been studied in detail,[2,11,12] whereas the efficiency E_{SSE} for sweeping through a single matching condition has not. Only recently did we realize that sweeping through both transitions is not necessarily more efficient than sweeping through only one, as shown in Figure 2. This illustrates the underlying physics that leads to a higher efficiency for the SSE and ASE as opposed to the ISE. For the moment, we define the ISE as a sweep through both SE matching conditions, whereas the SSE as through only one. From (4) we see that $0 < \mathscr{Q} < \infty$ and the maximum of E_{SSE} is 2 when $\mathscr{Q} \to \infty$, whereas that of E_{ISE} is only 0.6863 at $\mathscr{Q} = 1/\sqrt{2}$. $\mathscr{Q} \to \infty$ can be approached by an extremely slow sweep $\dot{\omega} \to 0$ (see (4)) and $E_{SSE} = \frac{P_S^0 - P_S^A}{P_S^0 - P_I} = 2$ which means that $P_S^A = -P_S^0$ when $P_I^0 = 0$, i.e., a full inversion of the electron polarization with respect to the effective field. Thus, when subsequently going through the second matching point, the nuclei are polarized toward the opposite direction, reducing the nuclear polarization; that is, the polarization is transferred from the surrounding nuclei back to the electron.

The theory is first compared to numerical simulations performed using the SpinEvolution[13] software, which is based on calculating the evolution of the density matrix. The available computing power limits the number of spins that can be used in the calculation. Thus, we performed the simulation on a system of a single electron interacting with nine nuclear spins, shown in Figure 2, and compared it to the theoretical values given by (5) and (6). The hyperfine interactions between the electron and the nine nuclei are assumed to be equal. The SpinEvolution simulation confirms the theoretical prediction that the ISE has an optimum $\mathcal{Q}$ or $\dot{\omega}$, whereas the SSE is always more efficient with higher $\mathcal{Q}$ or slower frequency sweep. Notice that the number of the nuclear spins in the simulated system is critical in studying DNP, because the electron polarization transfer efficiency increases when the number of nuclear spins increases. The maximum polarization transfer efficiency of the SSE can be larger than 1 for a system with many nuclear spins (as shown in Figure 2 for nine nuclear spins). This means that the electron polarization can be inverted with respect to the effective field as theory predicts. With more nuclear spins in the system, the SSE polarization transfer efficiency is approaching the theoretical prediction of the maximum 2.

One of the reasons for preferring the ISE is that to date pulsed-DNP experiments have been limited to low magnetic fields, where the EPR line width is broader than the nuclear Larmor frequency. In this case, a sweep from $-\infty$ to 0 only brings part of the electron spins through one matching condition, part through both, and the remainer through zero matching conditions. We can treat this situation by considering the entire EPR line as spin packets with spectral density $f(\Omega)$ and the polarization transfer of each spin packet is calculated separately. A finite sweep from ω_i to ω_f instead of from $-\infty$ transfers only a fraction of the electron polarization that is parallel to the effective field to the nuclei instead of the full electron polarization. The fraction of the polarization parallel to the effective field is given by

$$P_S^i(\Omega) = \pm P_S^0 \frac{\omega_{0S} + \Omega - \omega_i}{\sqrt{{\omega_{1S}}^2 + (\omega_{0S} + \Omega - \omega_i)^2}} \tag{7}$$

where $\omega_{0S} + \Omega$ is the electron Larmor frequency of a spin packet at frequency offset Ω and the sign of P_S depends on the sign of $\omega_{0S} + \Omega - \omega_i$.

Now we can write down the polarization transfer efficiency for any sweep and EPR line

$$\begin{aligned} E &= \int \mathrm{d}\Omega f(\Omega)(P_S^i(\Omega) - P_S^f(\Omega)) \\ &= \int_A \mathrm{d}\Omega f(\Omega)(P_S^i(\Omega) - P_I)E_{\mathrm{SSE}} \\ &\quad + \int_B f(\Omega)\mathrm{d}\Omega(P_S^i(\Omega) - P_I)E_{\mathrm{ISE}} \\ &= \int_A \mathrm{d}\Omega f(\Omega)(P_S^i(\Omega) - P_I)\frac{2\mathcal{Q}}{1+\mathcal{Q}} \\ &\quad + \int_B \mathrm{d}\Omega f(\Omega)(P_S^i(\Omega) - P_I)\frac{4}{(1+2\mathcal{Q})(1+\mathcal{Q}^{-1})} \end{aligned} \tag{8}$$

where the intervals A and B denote the spin packets going through a single or both matching points, respectively. Note that part of the spins that do not go through either of the matching points, induce no polarization transfer and contribute nothing to the integral. Here we have neglected the nonadiabatic process happening because of a sudden start and stop of the microwave pulse.

We immediately realize that the ASE deploying a narrow chirp pulse around one of the SE line[10] is exactly the case that the chirp pulse brings a fraction of the polarization through one of the matching conditions. Now that we have a clearer understanding of the spin dynamics induced by an arbitrary chirp pulse, we can better separate the ISE, SSE, and ASE, defined as follows. As illustrated in Figure 1, the ISE is a broad sweep bringing all of the electron spins through both SE matching conditions, e.g., the frequency offset Ω from $-\infty$ to $+\infty$, whereas the SSE is a broad sweep bringing most of the electron spins through one of the matching conditions, e.g., from $-\infty$ to 0, the center of the EPR line. Finally, the ASE is a narrow sweep around one of the SE lines.

Shown in Figure 3 are some representative experimental field profiles at different Rabi frequencies of the proton polarization build-up rate in a naphthalene single crystal doped with pentacene-d_{14}[14] polarized by triplet-DNP[12] at X-band. The photoexcited triplets of the pentacene-d_{14} guest molecules serve as the polarizing agent. The experimental sweep width was 22 G (~60 MHz) with $\dot{\omega} = 1.5$ G/μs (~4.2 MHz/μs) at three different Rabi fields ω_{1S} (details see below). The typical build-up time of the polarization in pentacene/napthalene crystals is about 5 h,[12] so a simple free induction decay (FID) NMR signal after 100 s DNP was used to monitor the initial build-up rate. This signal is directly proportional to the polarization transfer efficiency.

The plateau at the center of each field profile is because of the ISE effect, whereas around −30 MHz we find the SSE effect is maximal. These differences are especially prominent in Figure 3a. The data in Figure 3 are fit using the expression in (8), using the known parameters specified for the simulation. Specifically, we assume that the EPR line to be a Gaussian distribution with a 3 MHz standard deviation. We obtain an estimate of $\sqrt{M_2}/2\pi = 0.27$ MHz, compared to $\sqrt{M_2}/2\pi = 0.5$ MHz given by Eichhorn et al.[11] The discrepancy can be explained by the fact that we are using a much longer pulse, leading to decay of more triplets into their ground states in the middle of each DNP pulse. In addition, the level crossing becomes nonlinear (see eq 52 in Henstra et al.[2]) and can no longer be precisely described by the Landau–Zener theory. These factors also explain the nonperfect fit to the measured DNP field profiles.

The experimental results are in excellent agreement with our theoretical calculation. With a small Rabi frequency ω_{1S} (equivalent to a fast sweep, see eq 4), then the SSE is smaller than the ISE at the spectrum center. However, when ω_{1S} is large (equivalent to a slow sweep), then the SSE is more efficient than the ISE. The SSE is always more efficient when ω_{1S} increases (or sweep speed reduces), whereas the ISE has an optimum ω_{1S} (or sweep speed). These features are predicted by the theory and embodied in eqs 5 and 6 and Figure 2. Because the EPR line is symmetric, the frequency (field) with the optimal SSE efficiency is exactly a sweep to the center EPR frequency. For certain radicals, whose EPR spectrum is

asymmetric because of a g-anisotropy, there could be an offset for the optimum frequency (field) depending on the detailed shape of the spectrum.

Figure 4 summarizes the proton polarization build-up rate for the ISE and SSE as a function of $\frac{\sin^2\theta_A}{\cos\theta_A\dot{\omega}}$ that is proportional to $\mathcal{Q}$ (eq 4). Two sets of measurements with different sweep rates, $\dot{\omega}$ = 1.5 G/μs (same as Figure 3) and $\dot{\omega}$ = 1 G/μs, are combined. This further confirms the theoretical prediction that the ISE has an optimum whereas the SSE continues to improve with higher Rabi fields (higher θ) and slower sweep rates.

In addition, the field profile with a narrower sweep 10 G (28 MHz ~ EPR line width) with 1 G/μs (=2.8 MHz/μs) was recorded to demonstrate the theory to the ASE. The data agree well with the simulation, as illustrated in Figure 5.

To summarize, we have presented a theory for calculating the DNP transfer for any chirped pulse on or near an arbitrarily shaped EPR line. The theory is based on the Landau–Zener equations, and we verified its primary features with DNP measurements of the ^{1}H polarization build-up rate for the ISE, SSE, and ASE experiments.

Importantly, we showed that the ISE, SSE, and ASE are based on the same physical principles as the SE and NOVEL, where the energy levels of the electron and the surrounding nuclei are matched for mixing in the rotating frame. The ISE, SSE, and ASE employ adiabatic frequency swept chirped pulses (or magnetic field sweeps) and therefore can utilize the electron polarization of the entire EPR line, which is an advantage over NOVEL. The ramped-amplitude NOVEL (RA-NOVEL) experiment[15] also addresses this problem and yields improved enhancements. However, the ISE, SSE, and ASE require much less microwave power than the NOVEL and RA-NOVEL experiments.

The calculations also permit us to define borders among the ISE, SSE, and ASE. As we have seen, the ISE employs a broad frequency sweep, e.g., the frequency offset Ω from −∞ to +∞, where all of the electron spins transition through both matching conditions. The SSE also employs a broad sweep that brings most of the electron spins through one of the matching conditions, e.g., from −∞ to 0, the center of the EPR line. In contrast, the ASE is a narrow sweep around one of the SE lines. In an SSE or ASE, the majority of the electron spins transition through only one of the two matching points. Importantly, we have theoretically and experimentally demonstrated that, when the Rabi field ω_{1S} is strong and the sweep rate $\dot{\omega}$ is slow, then going through the matching point only once yields the optimum signal enhancement. This is because the electron polarization can be efficiently transferred to the nuclei (inverted in the extreme case) after going through the first matching condition. A subsequent passage through the second matching condition actually transfers negative polarization from the electrons to the surrounding nuclei or transfers nuclear polarization to the electron spin as shown by (1) and (2) when $2\mathcal{P} - 1 < 0$. This was confirmed using density matrix simulations and the program SpinEvolution. Furthermore, a comparison of (5) and (6) shows that an optimal SSE can be a factor of ~3 times (2/0.6863) more effective than an optimal ISE. This theoretical maximum may be approached when the EPR line is narrower than the nuclear Larmor frequency, a situation that exists in

experiments at high magnetic fields with trityl or BDPA as the polarizing agent. At low magnetic fields, in a X-band system, we currently observed a ~30% enhancement or the SSE compared to the ISE.

The system of pentacene-d_{14} doped naphthalene single crystal was chosen to verify the theory because of its exceptionally long nuclear spin–lattice relaxation time. However, in systems that are of more interest to DNP NMR, for instance biomolecular systems with trityl or BDPA radical as the poarizing agent, the nuclear T_1 needs to be taken into consideration. Still the more efficient polarization transfer of each SSE and ASE pulse compared to the ISE should lead to an overall higher enhancement, which was observed for SA-BDPA at 9.4 GHz and trityl at 9.4 and 94 GHz.[3,4,10] In addition, unlike pentacene where after each DNP pulse the electron is repolarized by the laser excitation following the triplet dark decay, the stable radicals rely on the T_{1e} for recovery of the polarization. Thus, the optimal DNP pulse repetition rate directly depends on the DNP mechanism. The electron polarization after an SSE sequence is in the *xy*-plane perpendicular to the magnetic field, yielding a zero electron polarization. However, an ISE pulse brings the electron polarization from parallel to antiparallel to the magnetic field *z*-direction. Therefore, in SSE experiments, it requires a shorter period for the electron spin polarization of stable radicals to recover to the $+z$ direction in comparison with the ISE. Thus, higher repetition rates and improved signal-to-noise is available from the SSE DNP experiment. One could consider returning the electron polarization to parallel to the magnetic field *z*-direction after each DNP (of any kind) pulse. This idea was suggested as a method to improve the execution of NOVEL.[16]

Furthermore, the coherence lifetime ($T_{1\rho}$ for these pulsed DNP mechanisms) of the electron was thus far not considered, which is justified for low field experiments, where the pulse is relatively short (several microseconds). However, at high fields where DNP MAS NMR experiments are performed, the sweep rate requires a careful optimization to balance the polarization transfer efficiency and the decoherence. In such cases the ASE is the preferred approach as only a narrow frequency sweep is required. Additionally, the fulfillment of the adiabatic condition $\frac{\pi\omega_1 S^2}{2|\dot{\omega}|} \gg 1$ needs to be taken into account because of the limited ω_1 at high frequency. For instance, we can currently only achieve $\omega_1/2\pi$ = 10 MHz with a gyrotron at 250 GHz and higher,[6,7,17,18] and therefore the sweep rate $\dot{\omega}$ has to be slower than 100 MHz/μs. However, with such a low ω_1 (much weaker than the nuclear Larmor frequency), most likely $Q < 1$ (see (4)), the polarization transfer efficiency is at the left side of the curves shown in Figure 2a. At, e.g., 250 GHz, the EPR line width of trityl is about 100 MHz[19] and in the rotating frame $T_{1\rho}$ is expected to be several tens of microseconds. Therefore, a slow sweep ASE should be preferred. However, the DNP efficiency as well as the adiabatic condition scales as $\omega_1{}^2$. This suggests the further development of more powerful gyrotrons and gyroamplifiers at sub THz frequencies to allow faster sweeps and perform more efficient chirped DNP.

EXPERIMENTAL METHODS

The experimental studies to verify the theory were performed with the triplet DNP system, a naphthalene molecular host crystal doped with a small amount of pentacene-d_{14} guest

molecules.[20] With a short laser pulse, pentacene is excited into a triplet state, which is strongly aligned because of the selection rules of the photoexcitation process.[21]

High quality crystals are grown using zone refined naphthalene doped with custom synthesized pentacene-d_{14} (ISO-TEC, Sigma-Aldrich Group) by a self-seeding Bridgman technique.[22] The pentacene concentration of the crystal used for the experiments was determined with optical transmission spectroscopy to be $(7.9 \pm 0.5) \times 10^{-5}$ mol/mol. The sample was introduced in an efficient home-built helium flow cryostat sitting between the pole pieces of a compact electromagnet. The cryostat is typically operated at 25 K during the DNP process. The pentacene molecules are photoexcited using a 556 nm laser (CNI HPL-556-Q 50) operating at 1 kHz.

A versatile home-built pulse X-band ESR system, operating at 9.3 GHz and synchronized to the laser was assembled to perform pulse DNP experiments.[14] A 10 turn saddle coil wound on a Teflon frame around the cavity provides the magnetic field sweep used for the DNP sequences. It can sweep up to ±40 mT with a rate of ~0.3 mT/μs. After DNP, the magnetic field is raised from 0.36 to 0.52 T, and the proton polarization is measured using a pulse NMR system based on a Spincore RadioProcessor card. This is possible because of the extremely long proton spin–lattice relaxation time in naphthalene of >800 h.[12] The long spin–lattice relaxation time is ideal for testing DNP theories and is one of the reasons for choosing this triplet system.

The relatively short lifetime of the triplet state requires a repetitive DNP experiment. Synchronized to the exciting laser pulse, is a strong microwave pulse of 10 μs length at a fixed frequency, which is applied while the field is adiabatically swept for performing the ISE, SSE, or ASE. Using a field sweep instead of a frequency sweep has the advantage that the microwave power stays constant over the sweep and is not modulated by the Q of the cavity.

ACKNOWLEDGMENTS

This work was supported by the National Institutes of Health through grants GM132997 and GM132079 to R.G.G. and the Swiss National Science Foundation through a grant to Y.Q. (No. P500PN_202639). We acknowledge the early contributions of Dr. T. V. Can on the ISE and SSE experiments.

REFERENCES

(1). Henstra A; Dirksen P; Wenckebach WT Enhanced Dynamic Nuclear Polarization by the Integrated Solid Effect. Phys. Lett. 1988, 134A, 134–136.

(2). Henstra A; Wenckebach WT Dynamic Nuclear Polarisation via the Integrated Solid Effect I: Theory. Mol. Phys. 2014, 112, 1761–1772.

(3). Can TV; Weber RT; Walish JJ; Swager TM; Griffin RG Frequency-Swept Integrated Solid Effect. Angew. Chem., Int. Ed. 2017, 56, 6744–6748.

(4). Can TV; McKay JE; Weber RT; Yang C; Dubroca T; van Tol J; Hill S; Griffin RG Frequency-Swept Integrated and Stretched Solid Effect Dynamic Nuclear Polarization. J. Phys. Chem. Lett. 2018, 9, 3187–3192.

(5). Delage-Laurin L; Palani RS; Golota N; Mardini M; Ouyang Y; Tan KO; Swager TM; Griffin RG Overhauser Dynamic Nuclear Polarization with Selectively Deuterated BDPA Radicals. J. Am. Chem. Soc. 2021, 143, 20281–20290.

(6). Hoff DE; Albert BJ; Saliba EP; Scott FJ; Choi EJ; Mardini M; Barnes AB Frequency Swept Microwaves for Hyperfine Decoupling and Time Domain Dynamic Nuclear Polarization. Solid State Nucl. Magn. Reson. 2015, 72, 79–89.

(7). Saliba EP; Sesti EL; Scott FJ; Albert BJ; Choi EJ; Alaniva N; Gao C; Barnes AB Electron Decoupling with Dynamic Nuclear Polarization in Rotating Solids. J. Am. Chem. Soc. 2017, 139, 6310–6313.

(8). Henstra A; Wenckebach W The Theory of Nuclear Orientation via Electron Spin Locking (NOVEL). Mol. Phys. 2008, 106, 859–871.

(9). Can TV; Walish JJ; Swager TM; Griffin RG Time Domain DNP with the NOVEL Sequence. J. Chem. Phys. 2015, 143, 054201.

(10). Tan KO; Weber RT; Can TV; Griffin RG Adiabatic Solid Effect. J. Phys. Chem. Lett. 2020, 11, 3416–3421.

(11). Eichhorn T; van den Brandt B; Hautle P; Henstra A; Wenckebach WT Dynamic Nuclear Polarisation via the Integrated Solid Effect II: Experiments on Naphthalene-h8 doped with Pentacene-d14. Mol. Phys. 2014, 112, 1773–1782.

(12). Quan Y; van den Brandt B; Kohlbrecher J; Wenckebach WT; Hautle P A Transportable Neutron Spin Filter. Nucl. Instrum. Methods Phys. Res. A 2019, 921, 22–26.

(13). Veshtort M; Griffin RG SPINEVOLUTION: A Powerful Tool for the Simulation of Solid and Liquid State NMR Experiments. J. Magn. Reson. 2006, 178, 248–282.

(14). Eichhorn TR; Haag M; van den Brandt B; Hautle P; Wenckebach WT; Jannin S; van der Klink J; Comment A An Apparatus for Pulsed ESR and DNP Experiments using Optically Excited Triplet States down to Liquid Helium Temperatures. J. Magn. Reson. 2013, 234, 58–66.

(15). Can TV; Weber RT; Walish JJ; Swager TM; Griffin RG Ramped-amplitude NOVEL. J. Chem. Phys. 2017, 146, 154204.

(16). Jain SK; Mathies G; Griffin RG Off-resonance NOVEL. J. Chem. Phys. 2017, 147, 164201.

(17). Nanni EA; Lewis SM; Shapiro MA; Griffin RG; Temkin RJ Photonic-Band-Gap Traveling-Wave Gyrotron Amplifier. Phys. Rev. Lett. 2013, 111, 235101.

(18). Nanni EA; Jawla S; Lewis SM; Shapiro MA; Temkin RJ Photonic-Band-Gap Gyrotron Amplifier with Picosecond Pulses. Appl. Phys. Lett. 2017, 111, 233504.

(19). Lumata L; Kovacs Z; Sherry AD; Malloy C; Hill S; van Tol J; Yu L; Song L; Merritt ME Electron Spin Resonance Studies of Trityl OX063 at a Concentration Optimal for DNP. Phys. Chem. Chem. Phys. 2013, 15, 9800–9807.

(20). Eichhorn TR; Haag M; van den Brandt B; Hautle P; Wenckebach WT High Proton Spin Polarization with DNP using the Triplet State of Pentacene-d14. Chem. Phys. Lett. 2013, 555, 296–299.

(21). Van Strien AJ; Schmidt J An EPR Study of the Triplet State of Pentacene by Electron Spin-echo Techniques and Laser Flash Excitation. Chem. Phys. Lett. 1980, 70, 513–517.

(22). Selvakumar S; Sivaji K; Arulchakkaravarthi A; Balamurugan N; Sankar S; Ramasamy P Growth of High-quality Naphthalene Single Crystals Using Selective Self-seeding Vertical Bridgman Technique (SSVBT) and its Characterization. J. Cryst. Growth 2005, 282, 370–375.

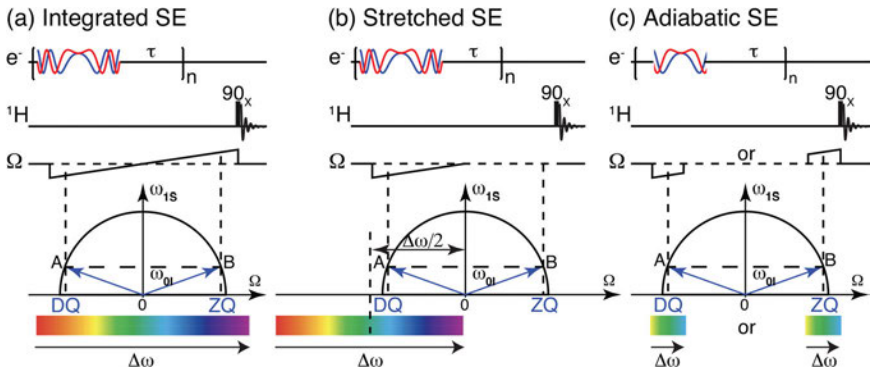

Figure 1.

Timing diagrams of the (a) ISE, (b) SSE, and (c) ASE in the rotating frame. (a) The ISE utilizes a broad microwave frequency sweep through both double quantum (DQ) and zero quantum (ZQ) matching conditions, e.g., $-\infty < \Omega < +\infty$. (b) The SSE also uses a broad sweep but only through one of the matching conditions, e.g., $-\infty < \Omega < 0$. (c) The ASE uses a narrow sweep around one of the SE matching conditions at $\omega_{0S} \pm \omega_{0I}$. The EPR line width is not reflected in the schematic drawings.

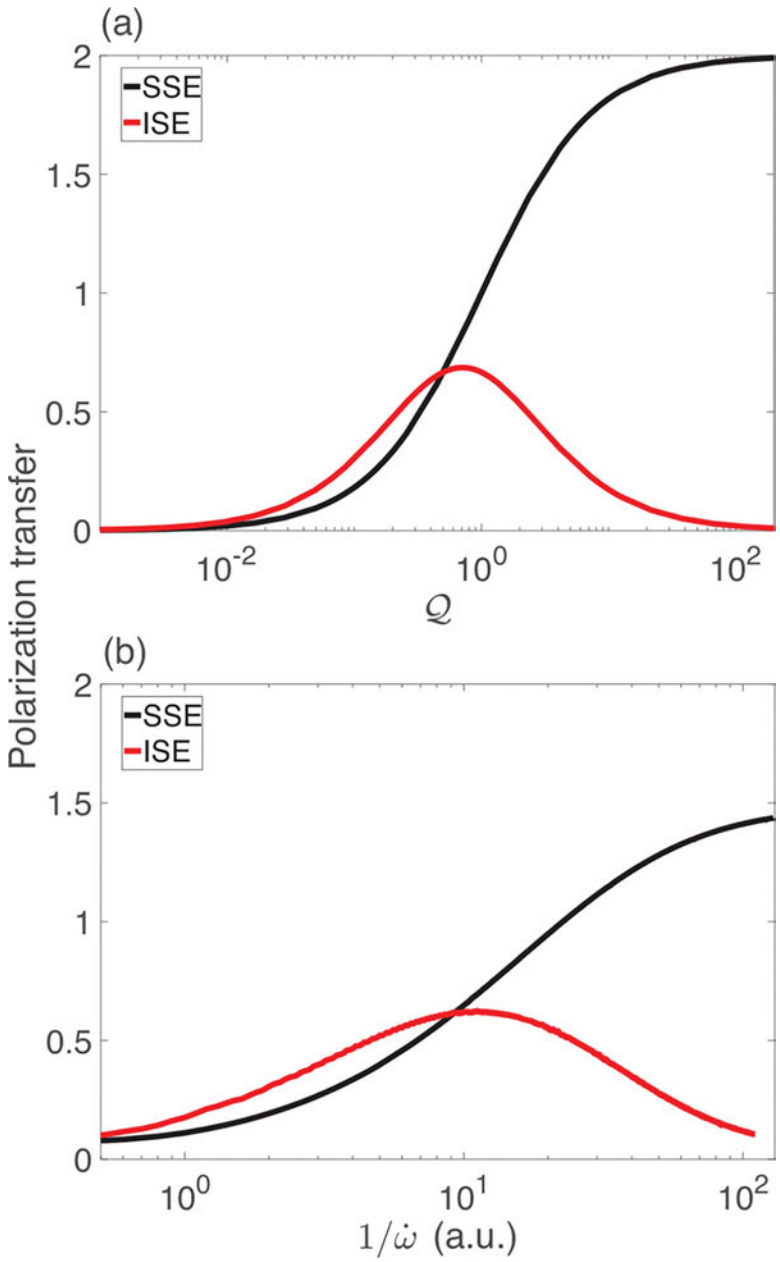

Figure 2.

(a) Electron polarization transfer efficiency for the SSE and ISE calculated from (5) and (6) as well as (b) the simulation using the SpinEvolution software. For the latter, a system of one electron spin interacting with nine nuclear spins is used, where the hyperfine interactions between the electron and each nuclear spin are identical. The theoretical calculation is plotted as a function of $\mathcal{Q}$, whereas the SpinEvolution simulation plot is plotted as a function of $1/\dot{\omega}$ (see (4)) as there are only a limited number (nine) of nuclear spins in the simulated system, hence no spectral density. The units for $1/\dot{\omega}$ in the simulation plot are arbitrary as they depend on the input hyperfine coupling strength. Both plots are with the horizontal axis on a logarithmic scale.

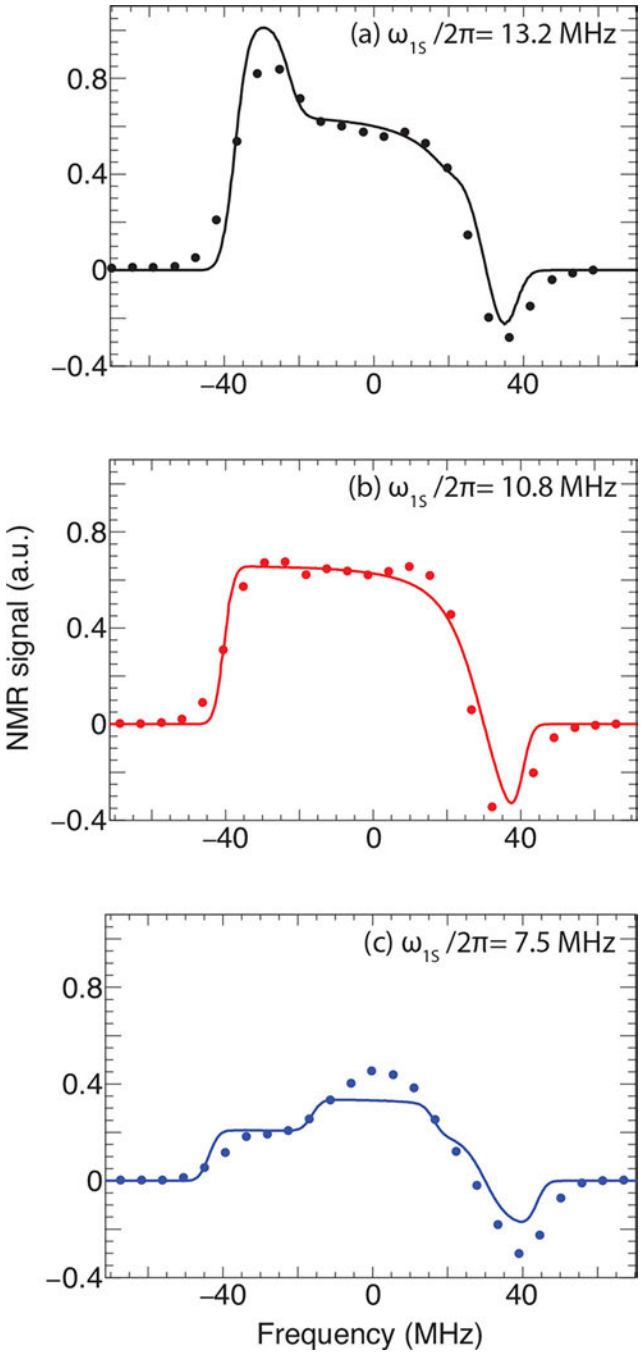

Figure 3.

Field profile of the proton polarization build-up rate in a naphthalene single crystal at $T = 25$ K, with different Rabi frequencies, ω_{1S}. The NMR signal after only 100 s DNP (compare to a typical 5 h rise time) is measured, which is linearly proportional to the build-up rate and the DNP efficiency. A total sweep width of 22 G (~60 MHz) with $\dot{\omega} = 1.5$ G/μs (4.2 MHz/μs) was employed and the horizontal axis indicates to the center of the sweep. The experimental data are fit to the theoretical model (eq 8), which yields the curves shown as solid lines.

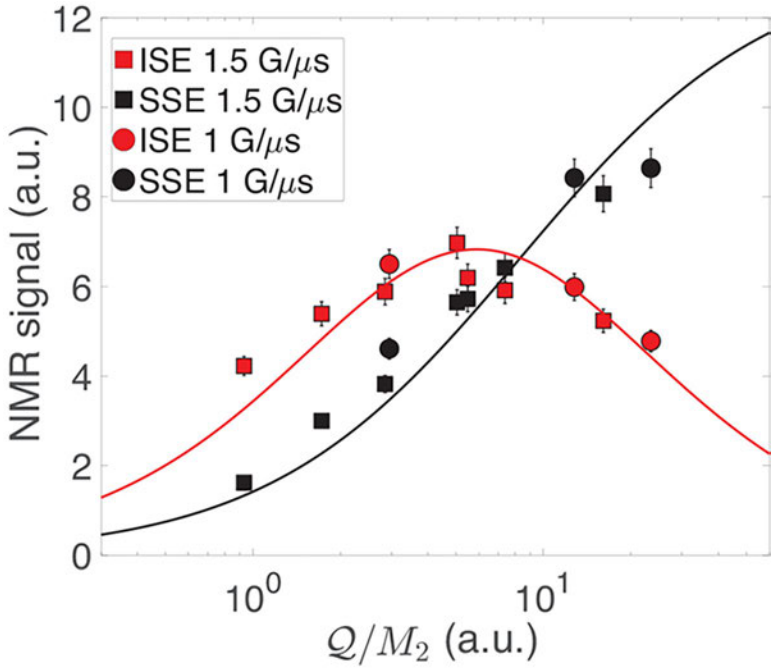

Figure 4.

Proton polarization build-up rate measured by NMR as a function of $\mathcal{Q}/M_2$ (see (4)) for the ISE (0 MHz in Figure 3) and SSE (−30 MHz in Figure 3), where two sets of data with $\dot{\omega} = 1.5$ G/μs and $\dot{\omega} = 1$ G/μs are combined. The solid lines are drawn as guides to the data.

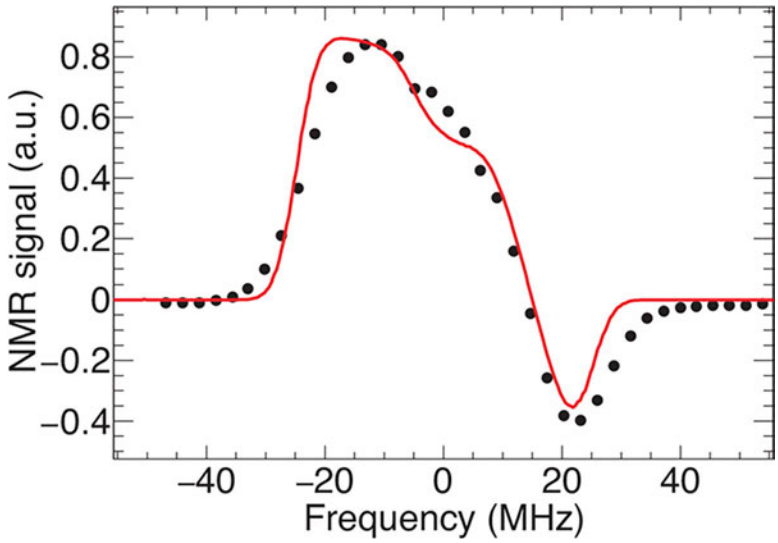

Figure 5.

DNP field profile of the ^{1}H polarization build-up rate in a naphthalene single crystal at T = 25 K measured by NMR with a 10 G (~28 MHz) field sweep (the sweep center is plotted as the horizontal axis) with $\dot{\omega}$ = 1 G/μs (2.8 MHz/μs). This experimental data are compared to the analytical calculation using eq 8 represented as the solid line.